Icarus **139**, 295–308 (1999)
Article ID icar.1999.6097, available online at http://www.idealibrary.com on IDEAL®

Numerous Weak Resonances Drive Asteroids toward Terrestrial Planets Orbits

A. Morbidelli and D. Nesvorný

Observatoire de la Côte d'Azur, B.P. 4229, 06304 Nice Cedex 4, France
E-mail: morby@obs-nice.fr

Received July 20, 1998; revised January 4, 1999

DEDICATED TO FABIO MIGLIORINI, WHOSE CONJECTURE WAS RIGHT.

A systematic exploration of the chaotic structure of the asteroid belt is presented, first taking into account only the perturbations provided by the four giant planets and then including also the effects of the inner planets. We find that both the inner belt ($a < 2.5$ AU) and the outer part of the main belt ($a > 2.8$ AU) are mostly chaotic. In the outer part of the belt, chaos is due to the presence of numerous mean-motion resonances with Jupiter and three-body resonances, Jupiter–Saturn–asteroid. In the inner belt, chaos is generated by mean motion resonances with Mars and three-body resonances, Mars–Jupiter–asteroid. Due to the chaoticity of the belt, asteroids tend to slowly migrate in eccentricity. This phenomenon of "chaotic diffusion" allows many bodies in the inner belt to become Mars-crossers. The number of asteroids leaking out from the inner belt is large enough to keep the population of Mars-crossing asteroids in steady state, despite of the short dynamical lifetime of the latter (∼25 Myr). We speculate that chaotic diffusion could have substantially eroded the high-eccentricity part of the asteroid belt, thus providing the impactors responsible for the Late Heavy Bombardment phase of the early Solar System. © 1999 Academic Press

Key Words: **asteroids; mean-motion resonances; mars-crossers.**

1. INTRODUCTION

Although the first examples of chaos in the Solar System were reported long ago (Giffen 1973, Scholl and Froeschlé 1974, 1975, Schubart 1978, Wisdom 1982, 1983), the systematic exploration of the chaotic structure of the asteroid belt is a science still in progress.

In two recent papers (Nesvorný and Morbidelli 1998a, Murray *et al.* 1998) the region between 3.1 and 4 AU was investigated by computing Lyapunov exponents for test particles initially placed on a regular grid in semimajor axis. This region appears to be almost densely filled by chaotic motions, which were identified with either ordinary mean-motion resonances with Jupiter or three-body mean-motion resonances with Jupiter and Saturn. It is worth reminding the reader that the former correspond to relations $m\dot{\lambda} + m_J\dot{\lambda}_J \sim 0$, and the second ones to $m\dot{\lambda} + m_J\dot{\lambda}_J + m_S\dot{\lambda}_S \sim 0$, where $\dot{\lambda}$, $\dot{\lambda}_J$, and $\dot{\lambda}_S$ denote the orbital frequencies of the asteroid, Jupiter, and Saturn, respectively, and m, m_J, and m_S are integers; $|m + m_J + m_s|$ is called the *order* of the resonance. With increasing eccentricity of the asteroid, the amplitudes of mean-motion resonances generally increase and the associated chaotic regions eventually overlap, making globally chaotic this part of the asteroid belt (Nesvorný and Morbidelli 1998a). The value of asteroid's eccentricity at which this occurs decreases with increasing semimajor axis, due to the proximity of Jupiter.

In the present paper, we extend the investigation of the chaotic structure to the inner asteroid belt. The motivation is provided by a recent paper which presents a revolutionary scenario for the origin of near-Earth asteroids: Migliorini *et al.* (1998) have shown that chaotic asteroids in the inner belt tend to migrate to higher eccentricities, until they become Mars-crossers; in turn, Mars-crossing asteroids move in semimajor axis under the effect of martian close encounters until they enter into a strong resonance that increases their eccentricities up to Earth-crossing values. From a quantitative viewpoint, the Mars-crossing asteroidal population should be considered as the main source reservoir of Earth-crossers; on the other hand, the asteroids leaking out from the inner belt sustain in a sort of steady state the Mars-crossing population, which otherwise would decay by 50% in about 25 Myr.

This paper is therefore structured as follows. In Section 2, we first extend the results of Nesvorný and Morbidelli (1998a) and Murray *et al.* (1998) by computing Lyapunov exponents of test particles initially placed on a regular grid in semimajor axis ranging from 2.1 to 3.24 AU, and which evolve under the gravitational forces of the four outer planets. In Section 3 we discuss the effects of the terrestrial planets on the chaotic structure of the inner belt. Section 4 is devoted to the analysis of chaotic diffusion: we correlate the main diffusion tracks with the chaotic regions detected in Section 3 and construct the estimate, anticipated in the Migliorini *et al.* paper, of the total number of bodies supplied by the inner asteroid belt to the Mars-crossing region. In the final discussion section we will speculate on the implications that chaotic diffusion might have on the long-term

0019-1035/99 $30.00
Copyright © 1999 by Academic Press
All rights of reproduction in any form reserved.

evolution of the asteroid belt, and on its possible relationship with the Late Heavy Bombardment recorded on the Moon.

2. ASTEROID CHAOS DUE TO THE FOUR GIANT PLANETS' PERTURBATIONS

To explore the chaotic structure of the asteroid belt, we have followed the procedure already adopted in Nesvorný and Morbidelli (1998a). We have set 5700 test particles on a regular grid in semimajor axis that ranges from 2.1 to 3.24 AU with a 2×10^{-4} AU spacing. The initial eccentricity was set equal to 0.1, while the initial inclination and phase angles were all set equal to zero with respect to the ecliptic and the Vernal point. The initial conditions for the outer planets corresponded to the Julian date 2449700.5. The test particles have been integrated over 2.3 Myr using a symmetric multistep method (Quinlan and Tremaine 1990), together with their variational equation in order to estimate the maximum Lyapunov exponent. The maximum Lyapunov exponent measures the ratio of divergence of nearby orbits and is a powerful indicator of chaos. It is mathematically defined as $\lim_{t\to\infty} \log \Delta(t)/t$, where $\Delta(t)$ is the norm of the variational vector at time t (Benettin *et al.* 1976). In the following we refer to the quantity $\log \Delta(t)/t$ as the "estimate of the Lyapunov exponent" at time t. The time step for the integrations was always less than 1% of the shortest orbital period, so that the integration method should not create spurious chaotic regions associated with low-order resonances between the time step and the dynamical frequencies. Tests have also been done changing the time step, to check the robustness of our Lyapunov exponent computation.

Figure 1 shows the estimate of the Lyapunov exponent at the end of the integration time span (in logarithmic scale) as a function of the initial semimajor axis. The figure shows several peaks which rise from a background level. The main peaks correspond to chaotic regions where the computation of the Lyapunov exponent has apparently reached its final limit value, as in the example of Fig. 2c. The background value of about $10^{-5.3} y^{-1}$ is dictated by the limited integration time span; increasing the latter, the background level would generally decrease (Figs. 2a and 2b). However, among the orbits for which the estimate of the Lyapunov exponent has not reached the limit value, we distinguish two cases: those for which the logarithm of the estimate linearly decreases with respect to the Logarithm of time (Fig. 2a) and those for which the time evolution of the Lyapunov estimate shows some cusps (Fig. 2b). The first orbits are the best candidates for being regular orbits. In the regions where these orbits are the vast majority (such as, for instance, in the inner asteroid belt) the background level of the Lyapunov estimate appears as a flat plateau. This is because regular regions are characterized by a continuous dependence of the results on the initial conditions. The orbits as in Fig. 2b, conversely, feel the existence of a local hyperbolic structure in the phase space; in other words, they are close to some resonance (see also Froeschlé *et al.* 1997). Although in principle they could be regular, in most realistic cases these orbits are chaotic, and the estimate of their Lyapunov exponent eventually tends to a positive limit value if computed on a longer time span. In the regions where these orbits are the majority (for instance beyond 2.85 AU), the background level of the Lyapunov estimate appears to be "rough": hyperbolicity breaks the continuous dependence of the result on the initial conditions. Therefore, although in the following we will concentrate only on the main peaks in Fig. 1, the shape of the background level is also an indicator of the local regular or chaotic structure of the belt.

Figure 1 shows that chaotic regions become denser with increasing semimajor axis. In fact, the location of mean-motion resonances of a given order become denser approaching Jupiter, and the sizes of the coefficients of the resonant harmonics increase with decreasing distance from the main perturber. This reflects on the number of visible peaks. We remind the reader that the height and width of each peak is roughly proportional to the the square root of the size of the coefficient of the corresponding resonant harmonic (see Murray and Holman (1997) for a more precise relationship).

We remark also that the peaks are located according to a peculiar structure: they form multiplets with a leading component at the center and secondary components on each side. This is a consequence of Jupiter and Saturn being close to the 5/2 mean-motion resonance. The combination $2\lambda_J - 5\lambda_S$, with λ_J and λ_S denoting the mean longitudes of Jupiter and Saturn, is an angle which circulates with negative derivative with a period of about 880 yr. This period is much longer than the typical asteroid orbital period, so that for any fixed integer numbers m, m_J, and m_S, the resonances given by the relations $m\dot{\lambda} + (m_J + 2k)\dot{\lambda}_J + (m_S - 5k)\dot{\lambda}_S \sim 0$ with different integer k, must be located close to each other (see also Murray *et al.* (1998)). The leading component of each multiplet is most often associated with the resonance of minimal order or with the resonance with $m_S - 5k = 0$. In Fig. 1, labels show the integers m_J m_S m of central components of most multiplets. Starting from a central component, the resonances with $k = 1, 2, \ldots$ (respectively, $k = -1, -2, \ldots$) are situated on the right (respectively, left) side of the central component if m is negative, and on the left (respectively, right) side if m is positive.

Figure 1 shows that most of the chaotic regions are associated with either ordinary mean-motion resonances with Jupiter ($m_S = 0$) or three body resonances Jupiter–Saturn–asteroid, confirming the results by Nesvorný and Morbidelli (1998a, 1998b) and Murray *et al.* (1998). The quoted papers also explain why these resonances produce positive Lyapunov exponents, so that we will not focus on this question again in this work. In Fig. 1 a few smaller peaks can be associated with three-body resonances Jupiter–Uranus–asteroid of low order. Conversely, no peak is apparently associated with a secular resonance. Secular resonances, in fact, should give Lyapunov exponents not larger than $\sim 10^{-6} y^{-1}$, because the Lyapunov exponent is typically of the same order as the inverse of the circulation/libration period of the resonant angle. We can therefore conclude that the most prominent chaotic structure of the asteroid belt is completely determined by mean-motion resonances. Among secular resonances, only the ν_6 resonance is visible. The latter is located at

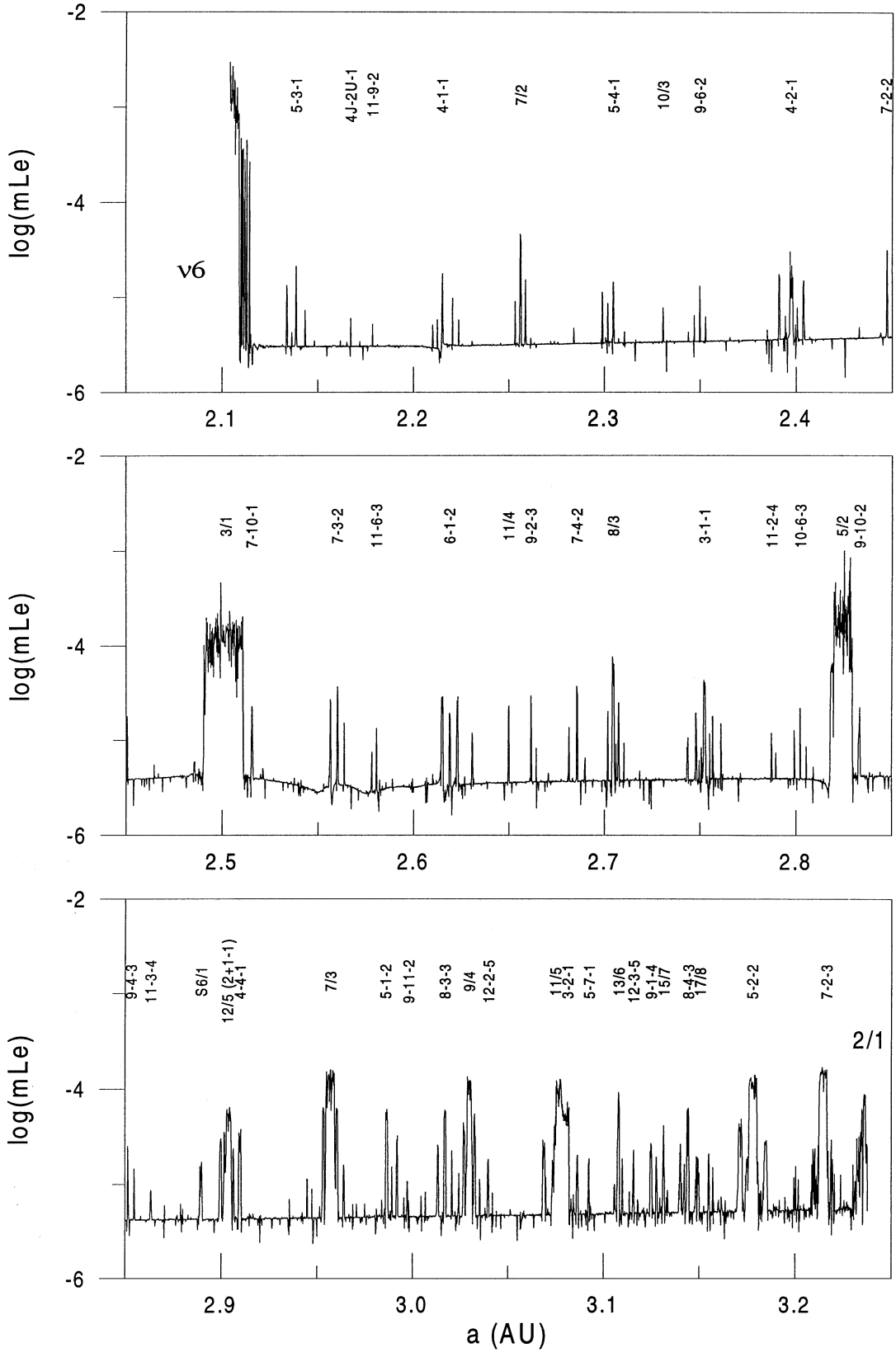

FIG. 1. The estimate of the maximum Lyapunov exponent (mLe) computed in 2.3 Myr integrations for test particles initially placed on a regular grid in semimajor axis, with initial eccentricity equal to 0.1 and initial inclination and phase angles all equal to 0. Only the gravitational perturbations provided by the four giant planets have been taken into account. The unit of mLe is y^{-1}. The peaks reveal the existence of narrow chaotic regions, associated with mean-motion resonances. The main resonances are indicated above the corresponding peaks. Labels m/n denote the ordinary m/n resonances with Jupiter, while labels $m\ n\ k$ denote the three-body resonances Jupiter–Saturn–asteroid (Nesvorný and Morbidelli 1998), which correspond to the equality $m\dot{\lambda}_J + n\dot{\lambda}_S + k\dot{\lambda} = 0$. Moreover, the label $S6/1$ denotes the $6/1$ resonance with Saturn and $4J - 2U - 1$ refers to the three-body resonance Jupiter–Uranus–asteroid corresponding to the equality $4\dot{\lambda}_J - 2\dot{\lambda}_U - \dot{\lambda} = 0$ ($\dot{\lambda}_U$ is the orbital frequency of Uranus). See text for comments on the chaotic structure of the belt.

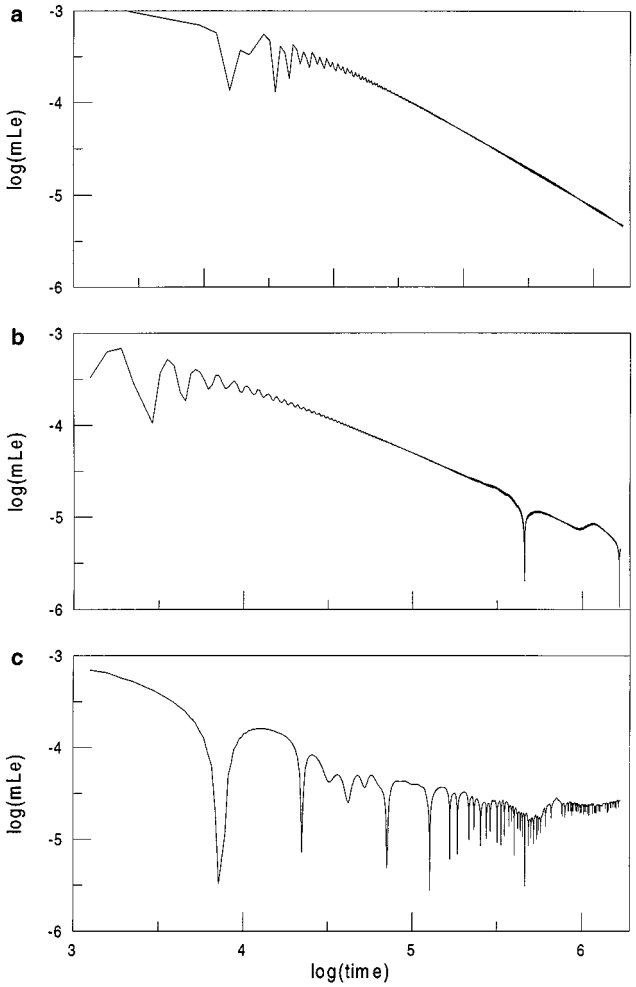

FIG. 2. The evolution of the estimate of the maximum Lyapunov exponent as a function of time. Unit of mLe is y^{-1}. (a) Regular orbit ($a = 2.1348$ AU in Fig. 1) for which log(mLe) decays linearly with log(time); (b) orbit ($a = 2.3426$ AU) which feels the close presence of a resonance, but for which the estimate of the maximum Lyapunov exponent has not yet attained his positive limit value; (c) chaotic orbit ($a = 2.139$ AU) for which the estimate of the maximum Lyapunov exponent has attained its limit value before the end of the integration time.

the inner border of the asteroid belt where the mean precession rate of the perihelion of the asteroid is in 1/1 resonance with the mean precession rate of that of Saturn. Most of the test particles in the ν_6 resonance escape to very large eccentricity and their integration is stopped before the 2.3 Myr limit. For this reason the estimates of their Lyapunov exponents are larger than $10^{-4}y^{-1}$.

The widths in semimajor axis of all mean-motion resonances, with the exception of those of order zero, increase with increasing asteroid eccentricity. As a consequence, the amount of chaos in the belt is enhanced at large eccentricity; the chaotic regions associated with different resonances may overlap making the belt globally chaotic. Beyond 3.1 AU this phenomenon has already been shown in Nesvorný and Morbidelli (1998a). In the inner belt, we have checked that increasing the initial asteroidal eccentricity to 0.2 just causes the overlapping of the resonances within the same multiplet, but distinct multiplets are still well separated. Therefore, the inner asteroid belt, in the approximation where only the outer planets are considered, appears to be characterized by chaotic bands, separated by large regular regions. Interestingly, these bands do not seem to be associated with evident gaps in the asteroid distribution. We will come back to this point in Section 4.

3. THE EFFECT OF THE INNER PLANETS ON ASTEROID CHAOS

The chaotic structure of the inner belt changes dramatically if the effects of the inner planets are also considered. Figure 3a shows the Lyapunov exponents in the inner belt resulting from a 2.3 Myr integration that includes all of the Solar System planets except Mercury. It can be directly compared with the top panel of Fig. 1 because the initial conditions of the integrated test particles are identical. The comparison shows in a striking

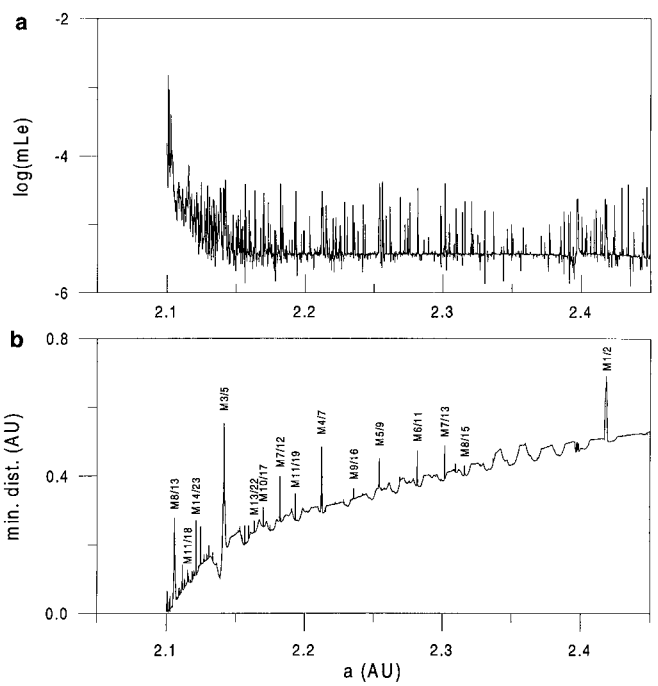

FIG. 3. (a) The same as Fig. 1 (top panel), but also taking into account the effects of the inner planets. Note that the inner belt, which appears to be basically regular when only the outer planets are considered, is densely filled by chaotic regions in a complete Solar System model. (b) The minimal approach distance to Mars as a function of the inital semimajor axis of the integrated test particles. Particles with $a > 2.106$ AU never approach Mars within 3 martian Hill spheres, which implies that their positive Lyapunov exponent is due to resonances and not to close encounters with the planet. The peaks reveal the location of the outer mean-motion resonances with Mars, the most important of which are labeled. Note that all mean-motion resonances with Mars correspond to peaks in the Lyapunov exponent distribution of panel (a).

way that the inner planets create a very large number of chaotic regions, which become denser with decreasing semimajor axis. Moreover, the background level of the Lyapunov exponent among the various peaks appears very irregular, in contrast with the flat shape that it had when only the outer planets were considered. As discussed in the previous section, this is an indication of a dense concentration of effective resonances and of the global chaoticity of the region. At semimajor axes smaller than 2.16 AU no background level is visible: for all test particles the computation of the Lyapunov exponent reaches a positive limit value within the integration time span. Notice that the Lyapunov exponent tends to increases with decreasing semimajor axis, until the ν_6 secular resonance is reached at 2.1 AU. The latter is moved to smaller semimajor axis with respect to Fig. 1a, because the presence of the inner planets slightly speeds up the precession rates of the particles' longitudes of perihelia.

The generally positive value of the Lyapunov exponent is *not* due to close encounters between the test particles and Mars. Figure 3b shows the minimal approach distance to Mars over the integration time as a function of the particles' semimajor axis: the minimal distance is larger than 1 martian Hill's sphere (7.25×10^{-3} AU) for all particles with $a \geq 2.103$ AU and larger than 3 martian Hill's spheres for $a \geq 2.106$ AU. Therefore, almost none of the test particles undergo close encounters with Mars, and their positive Lyapunov exponent must be due to resonances with the inner planets. To identify some of these, Fig. 3b is also very useful: the peaks that it shows reveal the presence of external mean-motion resonances with Mars. Only in these resonances, in fact, does the body avoid the closest approaches to the planet due to the well-known protection mechanisms that they provide (Malhotra 1996). Figure 3b labels the main external mean-motion resonances with Mars. Note that the peaks in Fig. 3b are always correlated with peaks in the Lyapunov exponent profile of Fig. 3a. Moreover, many small peaks appear in Fig. 3b for $a < 2.15$ AU, showing that high-order external mean-motion resonances with Mars accumulate in this region. This explains why the Lyapunov exponent is always positive in this semimajor axis range.

However, the external mean-motion resonances with Mars are not sufficient to explain the entire chaotic structure of the inner belt. In fact, there are many more peaks in the Lyapunov exponent profile than in the minimal approach distance curve. We have checked that most of these peaks are in fact related with three-body Mars–Jupiter–asteroid mean-motion resonances. As an example, Fig. 4 magnifies the 2.155–2.20 AU region and shows that 10 of the 13 peaks with Lyapunov exponent exceeding $10^{-5}y^{-1}$ are associated with either mean-motion resonances with Mars or three-body resonances Mars–Jupiter–asteroid. For the 3 remaining peaks we have not been able to identify with certainty the associated resonance. The mean-motion resonances with the Earth or Venus and the multibody resonances involving combinations of the orbital frequencies of the terrestrial planets do not seem relevant for the origin of chaos.

The resonance associations shown in Fig. 4 are not just chance alignments, but they have been verified in the numerical integrations. We report here two examples. Figure 5 shows, for a body located in the 1 1 −2 three-body resonance Mars–Jupiter–asteroid, the perfect correlation existing among the oscillations of the filtered semimajor axis, the librations of the critical angle $\sigma = \lambda_M + \lambda_J - 2\lambda$ (λ_M denoting the mean longitude of Mars) and the cusps in the evolution of the estimate of the Lyapunov exponent. This proves that the three-body-resonance dominates

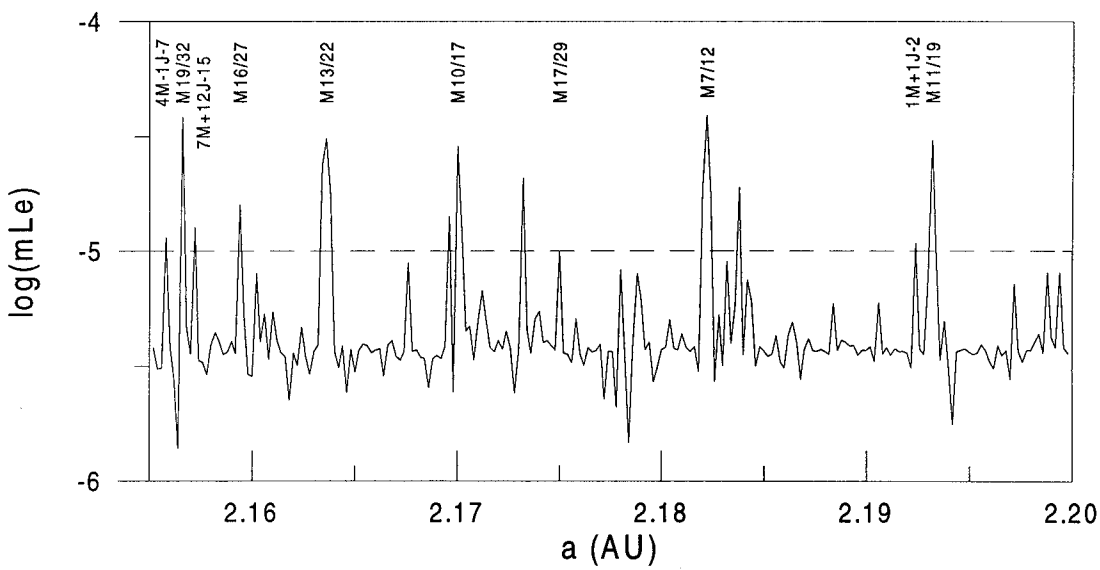

FIG. 4. Zoom of Fig. 3a in the 2.155–2.20 AU region. Ten of the 13 peaks exceeding $10^{-5}y^{-1}$ have been recognized to be associated with mean-motion resonances with Mars or three-body resonances Mars–Jupiter–asteroid. The labels Mn/m denote the n/m martian mean-motion resonances; the labels $lM + nJ + k$ denote the three-body resonances corresponding to the equality $l\dot{\lambda}_M + n\dot{\lambda}_J + k\dot{\lambda} = 0$ ($\dot{\lambda}_M$ denoting the orbital frequency of Mars).

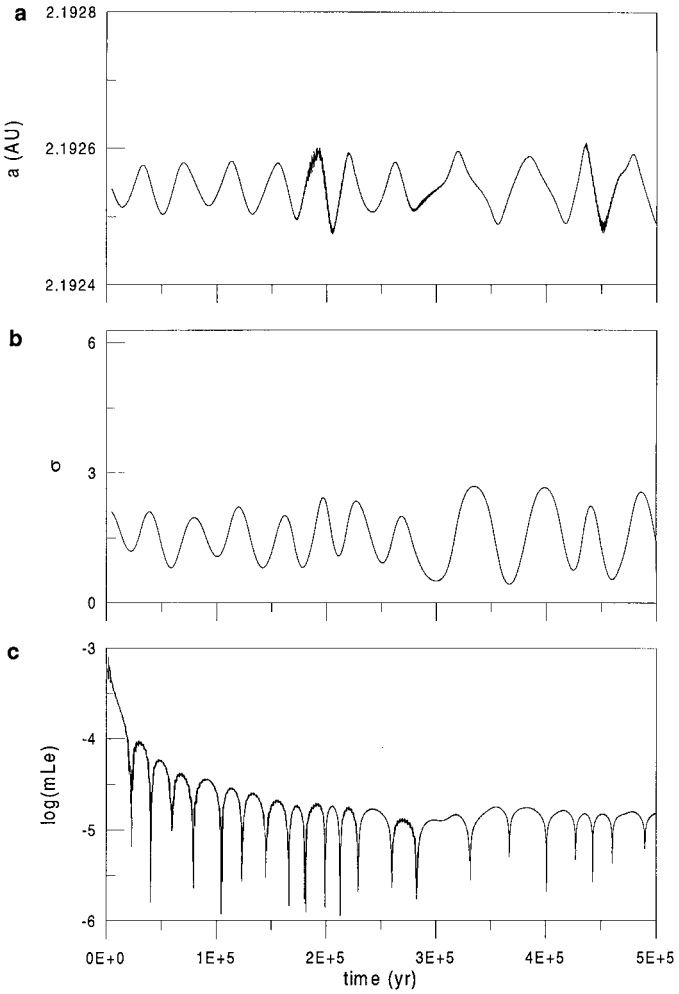

FIG. 5. Time evolution of (a) the filtered semimajor axis, (b) critical angle of the resonance $\sigma = \lambda_M + \lambda_J - 2\lambda$, and (c) estimate of the maximum Lyapunov exponent, for a test particle in the 1 1 −2 three-body resonance Mars–Jupiter–asteroid. The filtered semimajor axis is computed with the procedure explained in Nesvorný and Morbidelli (1998). Note the perfect correlation between the oscillations of the semimajor axis and the librations of σ. Also, the cusps in the evolution of the estimate of the maximum Lyapunov exponent are all related to the inversions of the motion of σ, which occur when the asteroid is close to the hyperbolic fixed point of the averaged resonant phase space.

the dynamical behavior of the body and determines its positive Lyapunov exponent. Figure 6 is analogous to Fig. 5 but refers to a body in the 16/27 mean-motion resonance with Mars. The critical angle shown in the middle panel is $\sigma_{3,8} = 16\lambda_M - 27\lambda + 3\varpi_M + 8\varpi$, where ϖ and ϖ_M denote, respectively, the longitudes of perihelia of the particle and of Mars. The correlation is not as good as the correlation shown in Fig. 5, because the resonances has several critical angles ($\sigma_{p,q} = 16\lambda_M - 27\lambda + p\varpi_M + q\varpi$ with $p + q = 11$ and positive p and q), and the oscillations of the semimajor axis as well as the cusps in the evolution of the estimate of the Lyapunov exponent can be related to the behavior of any of the critical angles. Still, Fig. 6 shows that the 16/27 mean-motion resonance strongly influences the motion of the body and the value of its Lyapunov exponent.

Because the mass of Mars is very small ($\sim 3.3 \times 10^{-7}$ solar masses) it might be astonishing that high-order martian mean-motion resonances or Mars–Jupiter–asteroid three-body resonances might be so relevant for asteroid motion. However, one should not forget that the asteroids in the inner belt come close to Mars, so that its small mass is compensated by the small distance. Moreover, as a general rule, the coefficients of high-order harmonics are not of order 1 in the usual units (Solar mass, Astronomical Unit, and Gaussian constant all set equal to 1). Finally, because the eccentricity of Mars is comparable to eccentricity of the considered asteroids, the coefficients of the harmonics of the different critical angles, which correspond to different relative powers of e_M and e (respectively, eccentricity of Mars and of the asteroid), are of the same order of magnitude, producing a strong time-modulation of the

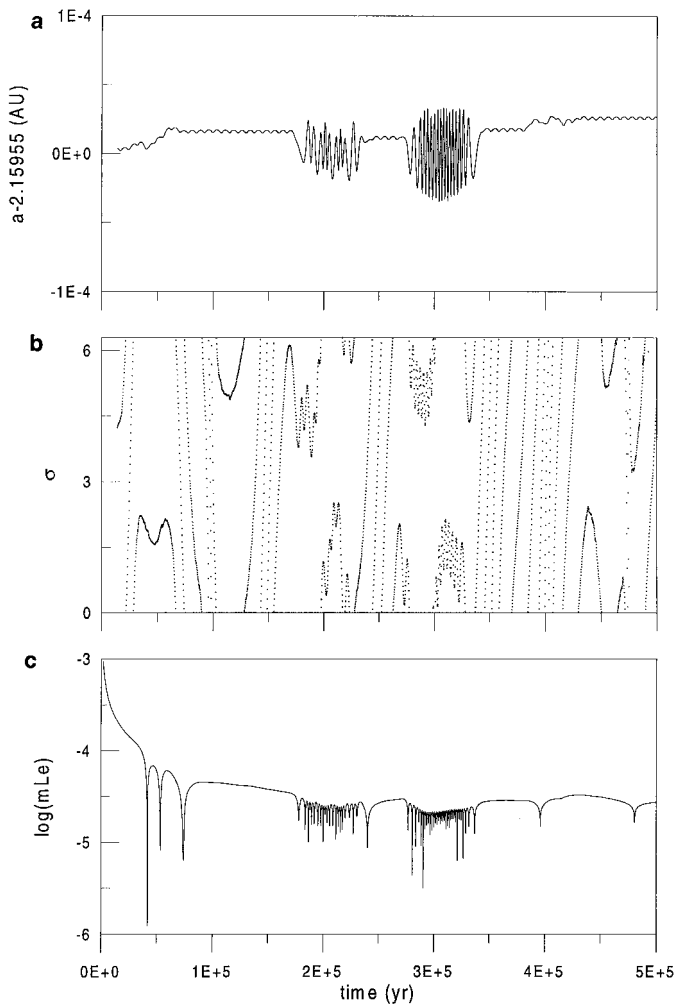

FIG. 6. The same as described in the legend of Fig. 5, but for a particle in the 16/27 mean-motion resonance with Mars. The angle σ is here $16\lambda_M - 27\lambda + 3\varpi_M + 8\varpi$. See text for comments.

amplitude of the resonances (see Morbidelli *et al.* (1995) for a theory on the modulation of mean-motion resonances). As an example, the coefficient of the harmonic $\cos(16\lambda_M - 27\lambda + 3\varpi_M + 8\varpi)$ of the 16/27 mean-motion resonance with Mars is $-5.6032 \times 10^7 \mu_M e_M^3 e^8/a_M$, where μ_M and a_M denote the mass and the semimajor axis of Mars. When both e and e_M are equal to 0.1, as is the case when the large semimajor axis oscillations are visible in Fig. 6, this makes the width of the 16/27 resonance equal to $\sim 1.6 \times 10^{-4}$ AU. To compare, the 15/4 mean-motion resonance with Jupiter, which is located very close to the 16/27 resonance with Mars, has the coefficient of its leading harmonic $\cos(15\lambda_J - 4\lambda - 6\varpi_J - 5\varpi)$ equal to $-6857\mu_J e_J^6 e^5/a_J$ which, for $e = 0.1$ and $e_J = 0.05$, gives the resonance a width of only 6.5×10^{-6} AU.

In general, the widths in semimajor axis of the resonances that we have identified are larger or of order 10^{-4} AU. Note that the test particles for which we have computed the Lyapunov exponent are 2×10^{-4} AU apart, so that in principle we could have missed a large number of peaks related to thinner resonances.

4. THE ORIGIN OF MARS-CROSSERS

The existence of so much chaos in the inner belt, as detected by our Lyapunov exponent computations, suggests that many asteroids could slowly increase their mean eccentricity and become Mars-crossers. To quantitatively study the relevance of this phenomenon and the time scales involved, no analytic estimate is accurate and reliable enough. Therefore, it is necessary to numerically integrate the evolution of a large number of bodies on time scales of order 10^8 yr.

Following a suggestion by F. Migliorini, we have numerically integrated a sample of 412 asteroids with osculating perihelion distance smaller than 1.8 AU, semimajor axis smaller than 2.5 AU, inclination smaller than 15°, and which are not Mars-crossers in the first 300,000 yr. The last property allows one to exclude from the sample population the "hidden Mars-crossers," namely those bodies that cross the orbit of Mars on a short time scale due to the secular oscillation of their orbital elements. The integrations have been done on several work stations using the swift_rmvs3 integrator, designed by Levison and Duncan (1994) as an extension of an algorithm originally invented by Wisdom and Holman (1991). The integrations covered time spans ranging from 100 to 300 Myr according to the used workstation speed. All planets have been taken into account, with the exception of Mercury.

To highlight small changes of the orbital elements over long time scales, we have numerically computed the asteroid's proper elements and their change over the integration time span. This has been done following a procedure very similar to the one illustrated in Morbidelli (1997): the orbital elements, output every 500 yr, are averaged using a running window that covers a 10 Myr time span. In other words, denoting generically the semimajor axis or the eccentricity by x, the proper value $x_p(t)$ is computed as

$$x_p(t) = \frac{1}{N} \sum_{t'=t-5\mathrm{Myr}}^{t'=t+5\mathrm{Myr}} x(t'), \tag{1}$$

where N denotes the number of output values of x over the considered time interval (20,000 in this case). A 10-Myr window is long enough to average out all important quasi-periodic oscillations of the osculating elements, and therefore the change over time of proper elements reveals non-quasi-periodic evolution, i.e., what is usually called *chaotic diffusion*. Conversely, regular bodies, which evolve on KAM tori (Kolmogorov 1954, Arnold 1963, Moser 1962) with only quasi-periodic oscillations of their osculating elements, have proper elements that are constant with time. For our purposes, we have computed proper elements every 10^5 yr, namely incrementing t in (1) by 10^5 yr steps from the initial value $t = 5$ Myr.

The initial proper semimajor axis and eccentricity of the integrated bodies, computed using formula (1) on the first 10 Myr of integration, are shown in Fig. 7. In the figure, red denotes bodies that will become Mars-crossers within the integration time. Only 3 bodies have a dynamical lifetime shorter than 10 Myr, so that their initial proper elements cannot be computed.

Figure 8 shows the evolution of the proper semimajor axis and eccentricity of the integrated bodies, as already presented in Migliorini *et al.* (1998). Only very few bodies have regular dynamics (those which appear as a dot in Fig. 8); the vast majority exhibits macroscopic diffusion in eccentricity—that is, a significant change of the proper eccentricity—in agreement with the conclusion of Section 3 that most of the bodies in the inner belt are chaotic. In Fig. 8, red denotes the evolution of the bodies when they are in the Mars-crossing regime, namely when their osculating perihelion distance becomes smaller than 1.665 during the time span covered by the computation of the corresponding proper elements. Under the effect of martian encounters, these bodies start to random-walk in semimajor axis, roughly following a curve of invariant Tisserand parameter with respect to Mars (see Valsecchi and Manara 1997), which makes their proper semimajor axis change with time. This change is moderate for shallow Mars-crossers and much bigger for deep Mars-crossers. Until the Mars-crossing status is reached, conversely, chaotic diffusion keeps the proper semimajor axis basically constant in the case of most of the bodies. This implies that the bodies diffuse in eccentricity always staying in the same mean-motion resonance or alternating among closely located resonances. Conversely, the few non-Mars-crossing asteroids that show macroscopic diffusion of proper semimajor axis must migrate along a chain of overlapping resonances.

4.1. *Diffusion Tracks*

We now analyze the diffusion process in more detail, trying to identify the main resonances that are involved. Figure 8 shows regions characterized by a large proper eccentricity variations

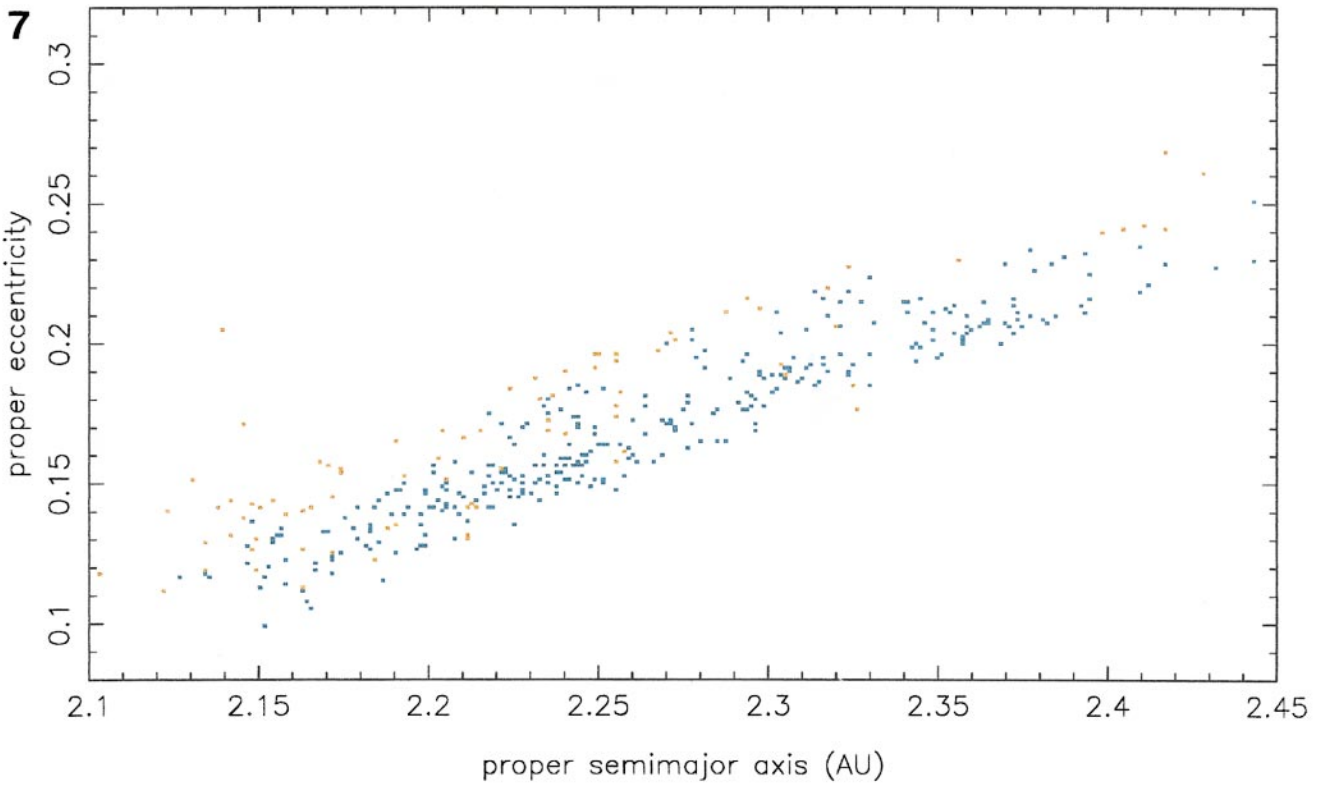
7
proper eccentricity
0.1
0.15
0.2
0.25
0.3
2.1
2.15
2.2
2.25
2.3
2.35
2.4
2.45
proper semimajor axis (AU)

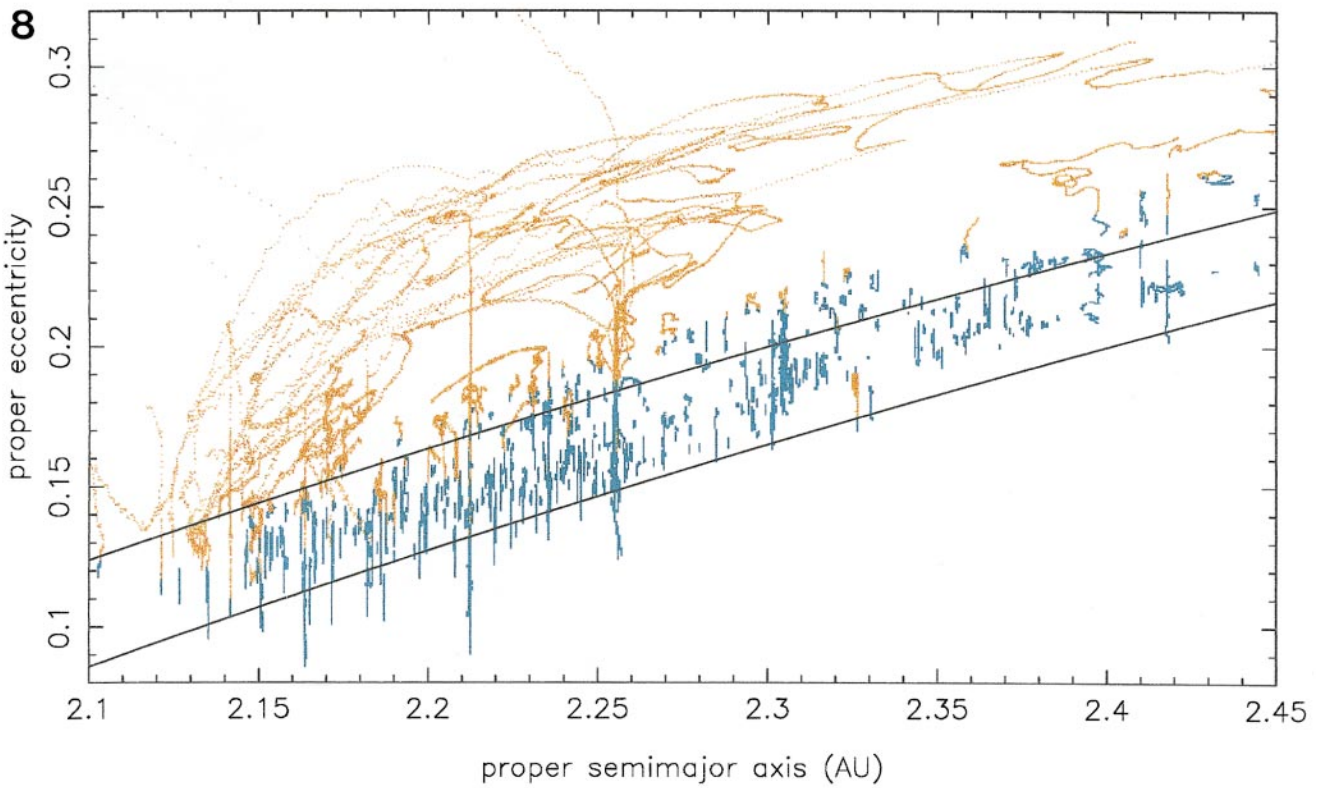
8
proper eccentricity
0.1
0.15
0.2
0.25
0.3
2.1
2.15
2.2
2.25
2.3
2.35
2.4
2.45
proper semimajor axis (AU)

and a background characterized by smaller, but still nonnegligible, eccentricity changes. To distinguish, we denote hereafter the first as the "main diffusion tracks" and the second as the "diffusion background."

The main diffusion tracks are: (i) at 2.256 AU, related to the almost coincident locations of the 7/2 mean-motion resonance with Jupiter and of the 5/9 mean-motion resonance with Mars (curiously, the latter seems to be more effective than the former); (ii) at 2.213 AU, related to the presence of the 4/7 mean-motion resonance with Mars; (iii) the region with semimajor axis smaller than 2.17 AU. This latter source region of Mars-crossers has been already identified by Morbidelli and Gladman (1998) but erroneously confused with the border region of the ν_6 secular resonance, where particles cross the orbit of Mars at the top of their secular eccentricity oscillation cycle. In reality, the mechanism responsible for the origin of Mars-crossers in this region is also chaotic diffusion driven by martian mean-motion resonances. As shown in Fig. 3, martian mean-motion resonances dominate this region, overlapping each other and giving origin to global chaos. The 3/5 mean-motion resonance with Mars at 2.142 AU is the most important among these resonances.

Moving to the outer part of the inner belt, the two remarkable diffusion tracks at 2.398 and 2.419 AU are, respectively, related to the $4\ -2\ -1$ three-body resonance Jupiter–Saturn–asteroid and to the 1/2 mean-motion resonance with Mars.

The diffusion background of Fig. 8 is also a real dynamical feature related to the dense presence of chaotic regions produced by martian perturbations. To illustrate this point, we compare in Fig. 9 the semimajor axis distribution of the Lyapunov exponent with the semimajor axis distribution of the proper eccentricity change. The latter is obtained by computing, for each test particle of Fig. 8, the maximal change of proper eccentricity *de* that occurs *before* being Mars-crosser. This provides a distribution of proper eccentricity changes *de* as a function of the initial proper semimajor axes. Both distributions in Figs. 9a and 9b have been smoothed using a suitable running window average; the profile in Fig. 9a was obtained by smoothing the Lyapunov exponent semimajor axis distribution illustrated in Fig. 3a. The comparison between Figs. 9a and 9b is striking. Not only the main peaks—associated with the main diffusion tracks discussed above—correspond, but also the minor peaks structuring the diffusion background appear to correspond to features of the Lyapunov exponent profile. In particular, in both panels peaks are particularly dense in the region with semimajor axes smaller than 2.25 AU, while they are less prominent and more separated in the more regular region between 2.3 and 2.4 AU. Moreover, both the Lyapunov exponent and the proper eccentricity changes tend to increase with decreasing semimajor axis in the region $a < 2.15$ AU. These features appear to explain the orbital distribution of Mars-crosser asteroids, whose number decreases with increasing semimajor axis between 2.1 and 2.5 AU (Migliorini *et al.* 1998). Only beyond 2.4 AU is the correspondence between the profiles in panels (a) and (b) poor, but this may be dictated by the scarce number of real asteroids that have been integrated in this region (see also Fig. 8).

This correspondence between the Lyapunov exponent distribution and the proper eccentricity change distribution is very important. The two distributions have been obtained using two completely different methods, namely the computation of Lyapunov exponents and the computation of proper elements, on the basis of evolutions computed numerically with two completely different integrators. This shows that our results are not an artifact of the adopted procedure or of the integration method; they reveal the *real* (surprising) dynamical structure of the asteroid belt.

4.2. The Escape Rate from the Inner Belt

We now present some statistics on the number of bodies that become Mars-crossers. Figure 10 shows the fraction of our integrated sample of bodies that has not become Mars-crosser, as a function of time. The decay of the non-Mars-crossing population indicates the escape rate from the inner belt. The integrated bodies have been divided in three sets according to their initial osculating perihelion distance, a division which clearly shows that the escape rate decreases for larger perihelion distance. This is not surprising, because the asteroids with smaller perihelion distance are statistically closer to the "brink," namely they have to diffuse less in eccentricity in order to cross the orbit of Mars. Remember however that the integrated bodies have been selected among those which do not become Mars-crosser in less than 300,000 yr due to a simple secular oscillation of the eccentricity.

In 25 Myr—the median dynamical lifetime of Mars-crossers (Migliorini *et al.* 1998)—about 21% of the bodies with $q <$ 1.78 AU, 14% of those with $1.78 < q < 1.79$ AU, and 6% of those with $1.79 < q < 1.80$ AU escape from the inner belt and start to cross the orbit of Mars. From 1997 Bowell's asteroid catalog (Bowell *et al.* 1994), and assuming the albedos reported in

FIG. 7. The proper semimajor axis and eccentricity computed over the first 10 Myr of evolution of the integrated asteroids in the inner belt. Red dots denote the objects that will become Mars-crossers before the end of the integration time.

FIG. 8. The evolution of the proper semimajor axis and eccentricity of the integrated bodies, whose initial values are shown in Fig. 7. Regular bodies appear as a dot, while chaotic bodies migrate, leaving a trace on the proper semimajor axis vs. proper eccentricity plane. The red color distinguishes the evolution of the bodies when they are in the Mars-crossing regime. Note that most of the bodies migrate in proper eccentricity keeping constant the proper semimajor axis before being Mars-crossers and move in semimajor axis after being Mars-crossers due to encounters with the planet. The two curves denote proper perihelion distances equal to 1.92 and 1.84 AU. A definite threshold separating Mars-crossing from non-Mars-crossing orbits cannot be defined with respect to proper perihelion distance, because it depends on the amplitude of eccentricity's secular oscillations. Note however that most of the bodies with proper perihelion distance larger than 1.84 AU are not Mars-crossers.

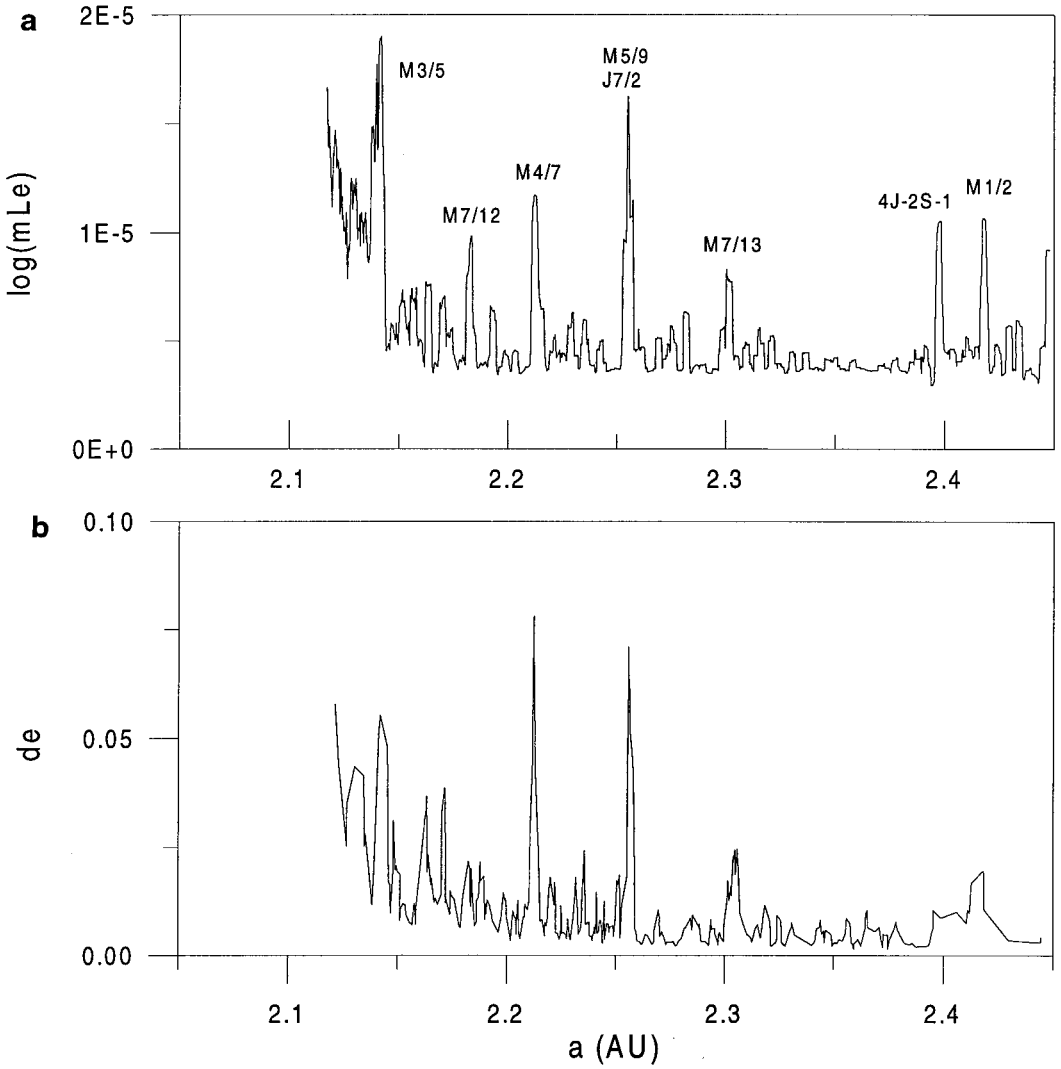

FIG. 9. A comparison between (a) the semimajor axis distribution of the Lyapunov exponent and (b) the semimajor axis distribution of the proper eccentrcity change de. Both distributions have been smoothed using an averaging running window. Note the remarkable similarity between the two profiles in panels (a) and (b). Labels denote the resonances associated with the main peaks. See text for discussion.

Table I of Migliorini *et al.* (1998), we estimate that the number of bodies larger than 5 km is 162 with $q < 1.78$ AU, 53 with $1.78 < q < 1.79$ AU, and 48 with $1.79 < q < 1.80$ AU.[1] This means that statistically $34 + 7 + 3 = 44$ bodies larger than 5 km should become Mars-crossers by leaking out from the inner belt in the next 25 Myr. This is about half of the flux necessary to keep the population of Mars-crossers with $2.1 < a < 2.5$ AU, and $i < 15°$ in steady state (∼90 per 25 Myr, according to Migliorini *et al.* (1998)). However, Fig. 8 shows that chaotic diffusion is important for the vast majority of bodies with proper perihelion distance smaller than 1.92 AU. According to the 1994 update of proper elements catalog (see Milani and Knežević 1994) about 800 asteroids in the inner belt larger that 5 km have proper perihelion distance smaller than this threshold (see Fig. 11), including part of the Flora and the Nysa families. Taking into account that the proper elements catalog lists only 3/5 of the objects larger than 5 km listed in 1997 Bowell's catalog for the inner belt, the real number should increase from 800 to about 1300. Therefore, it is very likely that the number of bodies leaking out from the inner belt will be enough to keep the number of Mars-crossers at the same present level for the next 25 Myr.

Conversely, this does not seem the case if longer time scales are considered. In our integrations, after the first 10 Myr, the escape rate decreases to about 10% of the population every 100 Myr, basically independently of the initial osculating perihelion distance (Fig. 10). Even considering that the population contains about 1000 bodies larger than 5 km, the number of bodies

[1] We limit our analysis to bodies larger than 5-km because for these bodies observational biases can be neglected in first approximation.

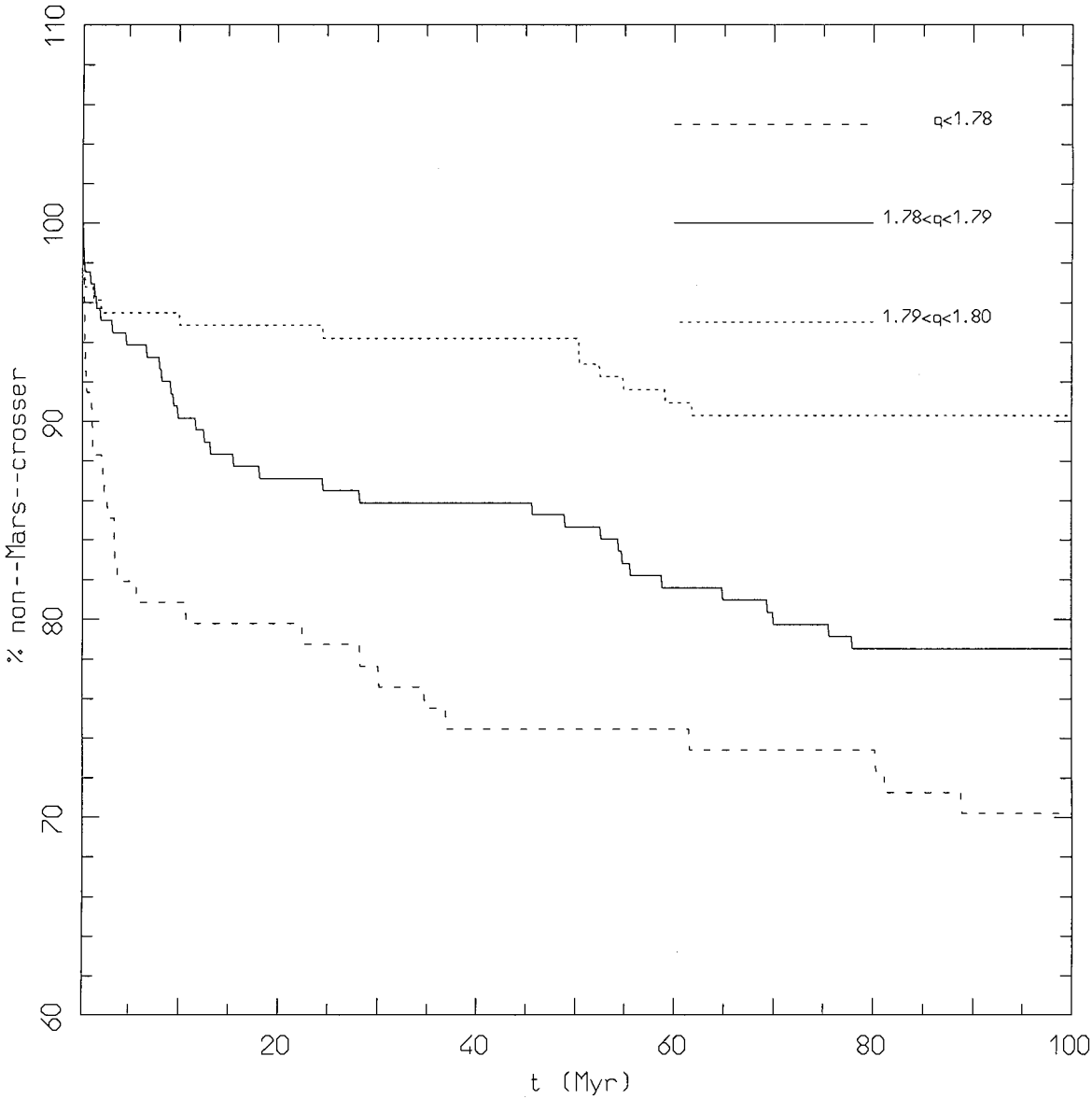

FIG. 10. The percentage of the integrated bodies that persist to be non-Mars-crossers as a function of time. The integrated population has been divided in three sets according to their initial osculating perihelion distance. The decay of the non-Mars-crossing population indicates the escape rate from the inner belt. Note that the escape rate is fast during the first ∼10 Myr and then stabilizes around 10% of the population escaping in 100 Myr.

that become Mars-crossers in 100 Myr seems to be four times smaller than the number of Mars-crossers that would be dynamically eliminated in the same time span, assuming for the latter the present "mortality" rate of ∼90 bodies/25 Myr. We do not believe that this implies that the Mars-crossers are not in steady state; it most probably means that our simulation is too simplistic to describe the real evolution of the asteroidal population on a 100-Myr time scale.

In fact, in our simulation the majority of the bodies in the main diffusion tracks escape in the first 10 Myr, leaving these regions depleted of objects, so that subsequently only the bodies in the "diffusion background" contribute to sustaining the Mars-crossing population, at a much lower rate. In reality the main diffusion tracks are not associated with gaps in the distribution of asteroids; this indicates that they must be resupplied with new objects on a ∼10-Myr time scale by some process(es) not taken into account in our simulation. Important processes that could bring new bodies to the large-eccentricity parts of the main diffusion tracks could be (*i*) diffusion from the low-eccentricity portion of the belt, (*ii*) injection into resonance by collisions and/or encounters among asteroids, (*iii*) migration in semimajor axis due to some nonconservative force, such as that given by the Yarkowsky thermal reemission effect (Burns *et al.* 1979, Rubicam 1995, Farinella *et al.* 1998) which could produce

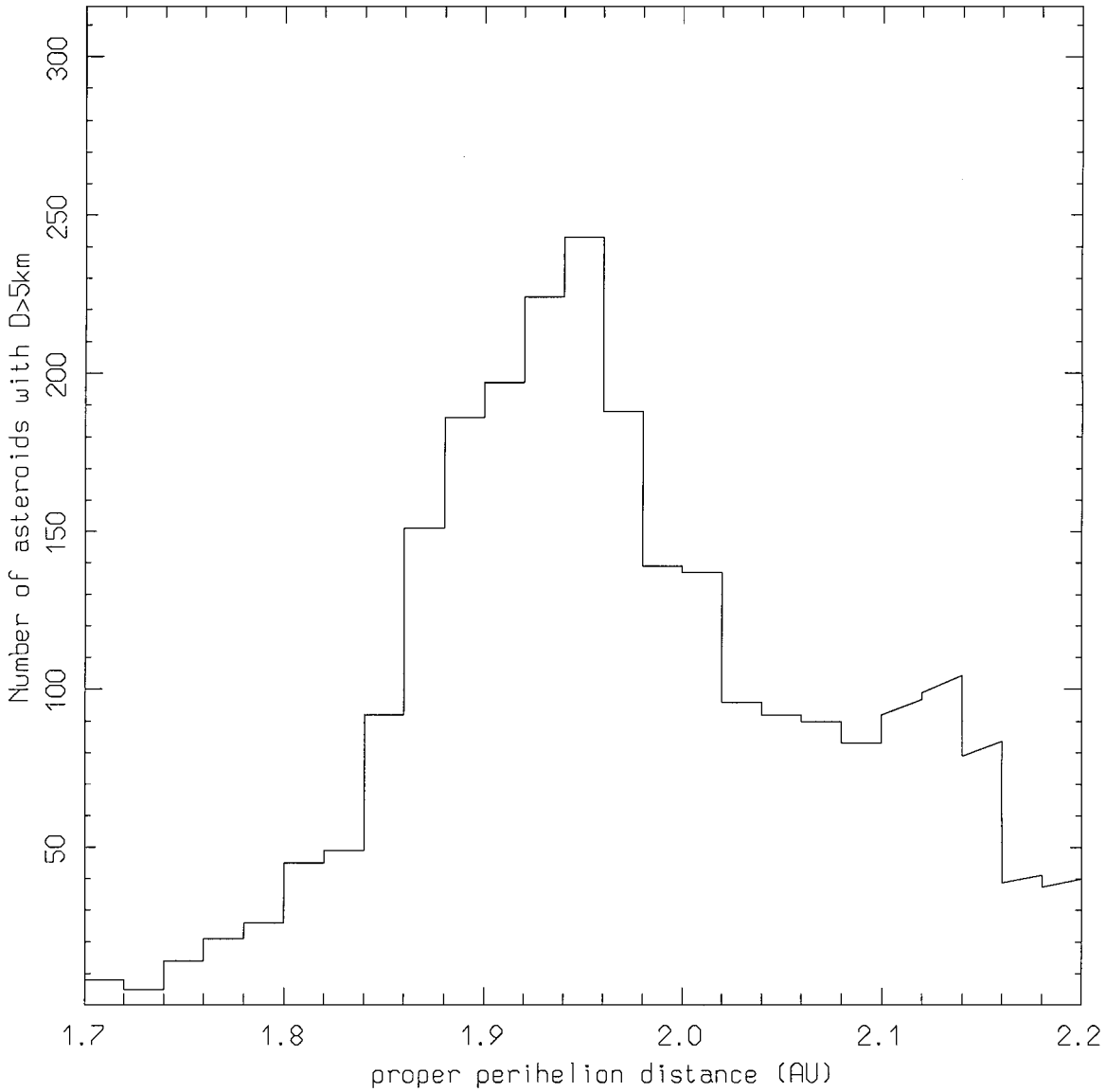

FIG. 11. The distribution of the asteroids larger than 5 km as a function of their proper perihelion distance. Note that the distribution is peaked at 1.95 AU, despite that most of the bodies with proper perihelion distance larger than 1.84 AU are not Mars-crossers (see Fig. 8). This peculiar distribution could be the combined result of the primordial excitation of the asteroid belt and of the substatial dynamical erosion of its high-eccentricity part.

a 0.005 AU mobility of multikilometer asteroids over 100-Myr time scales (Farinella and Vokrouhlický 1998). A quantitative analysis of these processes goes beyond the scope of this paper, but certainly their modeling should be included in a more realistic simulation of the origin of Mars-crossing asteroids.

5. CONCLUSIONS AND DISCUSSION

In this paper the chaotic structure of the asteroid belt in the 2.1–3.2 AU range is investigated. If only the outer planets are taken into account, chaos is mainly produced by mean-motion resonances with Jupiter and three-body resonances Jupiter–Saturn–asteroid. The 5/2 quasi-resonance between Jupiter and Saturn supplies a specific structure to the geography of asteroid resonances, producing clustered multiplets. The belt appears to be increasingly chaotic for larger semimajor axis; the inner belt ($a < 2.5$ AU) is basically regular, the resonance multiplets being well separated from each other.

The situation changes dramatically when the effects of the inner planets on asteroid dynamics are also taken into account. Mean-motion resonances with Mars and three-body resonances Mars–Jupiter–asteroid make the inner belt substantially chaotic, in particular in the 2.1–2.25 AU range. The existence of chaos is associated with an important diffusion in eccentricity, a process which concerns the vast majority of bodies with proper perihelion distance smaller than 1.92 AU. The diffusion in eccentricity

causes many inner belt asteroids to cross the orbit of Mars. We have shown that the number of 5-km bodies leaking out from the inner belt in the next 25 Myr should be enough to mantain the present number of Mars-crossers of similar size, despite the dynamical mortality of the latter. This is very important because Mars-crossers have been shown to be the main source reservoir of large Earth-crossing asteroids (Migliorini *et al.* 1998), so that sustaining the Mars-crossing population in steady state also sustains the Earth-crossing population. However, we have also shown that keeping the Mars-crossing population in steady state on longer time scales requires the participation of some processes not taken into account in our simulation, such as collisions or nonconservative forces.

Chaotic diffusion could have substantially eroded the high-eccentricity part of the asteroid belt over the age of the Solar System. Support that this must be so comes from the consideration that sustaining the Mars-crosser population requires the escape of about 100 bodies larger than 5 km every 25 Myr from the inner belt, namely 12,000 over the past 3 Gyr. This last figure is comparable to the total number of bodies larger than 5 km that are estimated to presently exist in the inner belt (Jedicke and Metcalfe 1998, Zappalà and Cellino 1996).

The distribution of asteroids with respect to proper perihelion or aphelion distances has a maximum at a value that is larger than the threshold leading to encounters with a planet. Figure 11 shows the distribution of the asteroids in the inner belt as a function of proper perihelion distance q_p. The histogram has been corrected by multiplying the number of bodies in the bins with $q_p > 2.1$ AU by $(2.5 - 2.1)/(2.5 - q_p)$, in order to roughly take into account that only the bodies in the semimajor axis range between q_p and 2.5 AU may have proper perihelion larger than q_p. The histogram peaks at about $q_p = 1.95$ AU, and decays at smaller perihelion distances, although Fig. 8 shows that most of the bodies with proper perihelion distance larger than 1.84 AU do not have encounters with Mars. The results of this paper show that chaotic diffusion should have substantially eroded the large eccentricity part of the belt. As a consequence, the original distribution of the asteroids, just after the primordial excitation of the belt, should have been substantially different from the present one, with many more asteroids in the 1.84–1.95 AU proper perihelion range.

In this scenario, moreover, it is reasonable to expect that the escape process from the asteroid belt has been much more intense in the past, immediately after the asteroid belt excitation, than at the present era. The inner planets and the Moon show evidence of a very intense Bombardment occurring in the first 0.5–1 Gyr after the planetary formation, a period usually called the *Late Heavy Bombardment* (see Neukum and Ivanov (1994) for a review). The origin of the late heavy bombardment is still an unsolved mystery. It was generally believed that it had been caused by the remnant planetesimals in the final stages of of the terrestrial planet formation, but recent work by Gladman *et al.* (1996) has shown that the dynamical decay of the number of bodies initially placed in the terrestrial planetary region is much faster (∼10 Myr) than the decay of the bombardment rate indicated by the cratering record (∼100 Myr). Results by Fernandez and Ip (1993) and more recently by Duncan and Levison (1997) show that the population in a "scattered disk" beyond Neptune decays with a rate similar to the one of the late heavy bombardment, suggesting a cometary origin of the latter. However, this is not very satisfactory because the D/H ratio in Earth's water is very different from that characterizing cometary ices (Bockelée-Morvan *et al.* 1998), which seems to exclude an important cometary component in the primordial bombardment of our planet. Neukum and Ivanov (1994) claim that the size distribution of the lunar craters during the late heavy bombardment seems also to point to an asteroidal origin of the projectiles. An intense primordial erosion of the asteroid belt could be an alternative source of projectiles which could explain the late heavy bombardment. Of course, this is for the moment only a working hypothesis.

REFERENCES

Arnold, V. I. 1963. Proof of A. N. Kolmogorov's theorem on the conservation of conditionally periodic motions with a small variation in the Hamiltonian. *Russian Math. Surveys* **18**, 9–36.

Benettin, G., L. Galgani, and J. M. Strelcyn 1976. Kolmogorov entropy and numerical experiments. *Phys. Rev. A* **14**, 2338–2345.

Bockelée-Morvan, D., D. Gautier, D. C. Lis, K. Young, J. Keen, T. Phillips, T. Owen, J. Crovisier, P. F. Goldsmith, E. A. Bergin, D. Despois, and A. Wootten 1998. Deuterated water in Comet C/1996 B2 (Hyakutake) and its implications for the origin of comets. *Icarus* **133**, 147–162.

Bowell E., K. Muinonen, and L. H. Wasserman 1994. A public-domain asteroid orbit database. In *Asteroids, Comets and Meteors* (A. Milani, M. di Martino, and A. Cellino, Eds.), pp. 477–481. Kluwer, Dordrecht.

Burns, J. A., P. H. Lamy, and S. Soter 1979. Radiation forces on small particles in the Solar System. *Icarus* **40**, 1–48.

Duncan, M. J., and H. F. Levison 1997. Scattered comet disk and the origin of Jupiter family comets. *Science* **276**, 1670–1672.

Farinella, P., and D. Vokrouhlický 1998. Semimajor axis mobility of asteroidal fragment. *Science* **283**, 1507–1510.

Farinella, P., D. Vokrouhlický, and W. K. Hartmann 1998. Meteorite delivery via Yarkovsky orbital drift. *Icarus* **132**, 378–387.

Fernandez, J. A., and W. H. Ip 1983. On the time evolution of the cometary flux in the region of the terrestrial planets. *Icarus* **54**, 377–387.

Froeschlé, C., E. Lega, and R. Gonczi 1997. Fast Lyapunov indicators. Application to asteroidal motion. *Celest. Mech. Dynam. Astron.* **67**, 41–62.

Giffen, R. 1973. A study of commensurable motion in the asteroid belt. *Astron. Astrophys.* **23**, 387–403.

Gladman, B., J. A. Burns, M. Duncan, P. Lee, and H.F. Levison 1996. The exchange of impact ejecta among terrestrial planets. *Science* **271**, 1387–1392.

Jedicke, R., and T. S. Metcalfe 1998. The orbital and absolute magnitude distributions of main belt asteroids. *Icarus* **113**, 245–260.

Kolmogorov, A. N. 1954. Preservation of conditionally periodic movements with small change in the Hamiltonian function. *Dokl. Akad. Nauk SSSR* **98**, 527–530.

Levison, H. F., and M. Duncan 1994. The long term dynamical behavior of short period comets. *Icarus* **108**, 18–36.

Malhotra, R. 1996. The phase space structure near Neptune resonances in the Kuiper Belt. *Astron. J.* **111**, 504–512.

Migliorini, F., P. Michel, A. Morbidelli, D. Nesvorný, and V. Zappalà 1998. Origin of multikilometer Earth and Mars-crossing asteroids: A quantitative simulation. *Science* **281**, 2022–2024.

Milani, A., and Z. Knežević 1994. Asteroid proper elements and the chaotic structure of the asteroid main belt. *Icarus* **107**, 219–254.

Morbidelli, A. 1997. Chaotic diffusion and the origin of comets from the 2/3 resonance in the Kuiper belt. *Icarus* **127**, 1–12.

Morbidelli, A., and B. Gladman 1998. Orbital and temporal distribution of meteorites originating in the asteroid belt. *Meteor. Planet. Sci.* **33**, 999–1016.

Morbidelli, A., V. Zappalá, M. Moons, A. Cellino, and R. Gonczi 1995. Asteroid families close to mean-motion resonances: Dynamical effects and physical implications. *Icarus* **118**, 132–154.

Moser, J. 1962. On invariant curves of area-preserving mappings of an anulus. *Nachr. Akad. Wiss. Göttingen Math. Phys.* **2**, 1–23.

Murray, N., and M. Holman 1997. Diffusive chaos in the outer belt. *Astron. J.* **114**, 1246–1259.

Murray, N., M. Holman, and M. Potter, 1998. On the origin of chaos in the Solar System. *Astron. J.* **116**, 2583–2589.

Nesvorný, D., and A. Morbidelli 1998a. Three-body mean-motion resonances and the chaotic structure of the asteroid belt. *Astron. J.* **116**, 3029–3037.

Nesvorný, D., and A. Morbidelli 1998b. An analytic model of three-body mean-motion resonances. *Celest. Mech. Dynam. Astron.*, in press.

Neukum, G., and B. A. Ivanov 1994. Crater size distributions and impact probabilities on Earth from lunar, terrestrial-planet and asteroid cratering data. In *Hazards Due to Comets and Asteroids* (T. Gehrels, Ed.), pp. 359–416. University of Arizona Press, Tucson.

Quinlan, G. D., and S. Tremaine 1990. Symmetric multistep methods for the numerical integration of planetary orbits. *Astron. J.* **100**, 1694–1700.

Rubincam, D. P. 1995. Asteroid orbit evolution due to thermal drag. *J. Geophys. Res.* **100**, 1585–1594.

Scholl, H., and C. Froeschlé 1974. Asteroidal motion at the 3/1 commensurability. *Astron. Astrophys.* **33**, 455–458.

Scholl, H., and C. Froeschlé 1975. Asteroidal motion at the 5/2, 7/3, and 2/1 resonances. *Astron. Astrophys.* **42**, 457–463.

Schubart, J. 1978. New results on the commensurability cases of the problem Sun–Jupiter–Asteroid. In *Dynamics of Planets and Satellites and Theories of Their Motion* (V. Szebehely, Ed.), pp. 137–143. Reidel, Dordrecht.

Valsecchi, G. B., and A. Manara 1997. Dynamics of comets in the outer planetary regions. *Astron. Astrophys.* **323**, 986–998.

Wisdom, J. 1982. The origin of the Kirkwood gaps: A mapping for the asteroidal motion near the 3/1 commensurability. *Astron. J.* **87**, 577–593.

Wisdom, J. 1983. Chaotic behavior and the origin of the 3/1 Kirkwood gap. *Icarus* **63**, 272–289.

Wisdom, J., and M. Holman 1991. Symplectic maps for the N-body problem. *Astron. J.* **102**, 1528–1538.

Zappalà, V., and A. Cellino 1996. Mainbelt asteroids: Present and future inventories. In *Completing the Inventory of the Solar System* (T. W. Reltig and J. Hahn, Eds.), ASP Conf. Series, Vol. 107, pp. 29–44, San Francisco.